Tomography of molecular nanographene double layers using scanning tunneling microscopy

C. Seifert,[1] D. Skuridina,[1,2] X. Dou,[3] K. Müllen,[3] N. Severin,[1,*,†] and J. P. Rabe[1,*,‡]
[1]*Department of Physics, Humboldt-Universität zu Berlin, Newtonstr. 15, D-12489 Berlin, Germany*
[2]*Department of Physics, M.V. Lomonosov Moscow State University, Leninskie Gory, Moscow 119991, Russia*
[3]*Max Planck Institute for Polymer Research, Ackermannweg 10, 55128 Mainz, Germany*
(Received 4 September 2009; revised manuscript received 3 November 2009; published 21 December 2009)

Double layers of a nanographene with defined molecular structure have been self-assembled at the interface between a molecular solution and the basal plane of graphite. Bias-dependent scanning tunnel microscopy allowed nondestructive imaging of the first or the second or both layers. While the first molecular layer can be well recognized at low negative or high positive sample biases, it is the other way around—at high negative or low positive sample biases—for the second molecular layer. This is attributed to the dependence of the resonant tunneling conditions for the molecules in the first and second layers on the position of the molecules within the tip-substrate gap. The effect may be used for a nanotomography of molecular multilayers.

DOI: 10.1103/PhysRevB.80.245429 PACS number(s): 07.79.Cz

Scanning tunneling microscopy (STM) is a powerful tool for high-resolution imaging of single molecules and the in-plane structure of molecular monolayers on conductive surfaces.[1,2] However, direct nondestructive molecular imaging of multilayers with a molecular resolution in the vertical direction remains a challenge.[3–8] In certain cases Moiré patterns from different lattices in subsequent molecular layers may be analyzed.[7] In others one can follow layer images as a function of layer thickness[3,4,6,8] or an underlying molecular layer may be imaged by pushing the upper layer around with the STM tip.[5,8] Here we report nondestructive imaging of the first or the second or both layers of a molecular bilayer depending on the particular tunneling conditions.

We employed a disk-type polycyclic aromatic hydrocarbon **1** (Fig. 1), which due to its size can be considered as nanographene that owes its solubility to the attachment of soft alkyl chains. Further, the "*para*-substitution" with a donor and acceptor group gives rise to a strong in-plane dipole moment. This dipole moment is important for the stacking within discotic mesophases and also for the deposition of the molecule on surfaces in the presence of electromagnetic fields.[9] On graphite, nanographene **1** forms double layers, which can be imaged at submolecular resolution. Since the first and the second layers are distinctly different as we will show in the following, **1** proves as an ideal object for the present STM study. Full description of synthesis and characterization of **1** will be published elsewhere.[10]

STM imaging was performed at the interface between the basal plane of graphite and organic solutions[2] with a home-built beetle-type instrument.[11] Nanographene **1** [Fig. 1(a)] was dissolved in trichlorobenzene at a concentration of 50 mg/l. A droplet of the solution was applied to freshly cleaved highly oriented pyrolytic graphite (HOPG). STM imaging was performed with tips of a mechanically cut Pt/Ir wire at substrate biases $\pm(0.5-1.3)$ V with the tip at ground potential and set-point currents 30–100 pA. The highest set-point current for stable imaging was typically selected for each experiment; the reason for this choice will be clarified in the discussion of the results.

Nanographenes have been observed to be generally donor type, i.e., their highest-occupied molecular orbital (HOMO) is located closer to the Fermi level than the lowest-unoccupied molecular orbital (LUMO).[13–15] For this reason they are typically imaged at negative sample biases, where resonant tunneling through the HOMO can be achieved. We therefore present first the results of STM imaging of nanographene **1** at negative sample biases, which reveals two different types of molecular packing (Fig. 2): regular oblique molecular arrangement (I) and arrays of dimers (II). They typically coexist with noisy image areas, which we attribute to a disordered molecular phase. The boundaries of the ordered islands are typically mobile and the structure of the dimer phase exhibits characteristic defects, particularly missing rows. The average area per molecule is undistinguishable for the two phases (3.25 ± 0.03 nm^2 for a regular dimer structure and 3.2 ± 0.1 nm^2 for the oblique structure). Dimers appear to be higher on the height images recorded at large negative sample bias in comparison with the oblique structures. Careful analysis of the dimer images reveals overlapping of the dimers with the obliquely packed molecules, implying the formation of a double layer. We conclude that the molecular layer with the larger number of defects assembles on top of an almost defect-free layer, i.e., the dimer structure forms on top of the oblique layer. Matching of the unit-cell areas of both structures implies furthermore epitaxial growth of dimers on the oblique layer. The assumed donor type of the molecules is consistent with the current-voltage dependencies measured on both types of structures [Figs. 2(b) and 2(c)], which exhibit higher tunneling currents at negative sample bias, implying a smaller energy gap of the HOMO to the Fermi level than that of the LUMO.

The visibility of the layers in the STM images changes drastically upon variation in the applied bias. More precisely, the reduction in the negative sample bias leads to gradual vanishing of the dimer structure and the underlying regular oblique molecular layer becomes more pronounced [Figs. 2(c) and 2(d); Figs. 3(a) and 3(b) and Ref. 12]. Comparison of the images of the dimer layers recorded before bias reduction and after its increase back to the original value reveals that the images are identical, i.e., defects such as missing molecules are fully recovered after the bias circle.[12] This observation implies that the structure of the dimer layer remains unperturbed during bias variation and just its visibility varies. Moreover, the observed gradual vanishing of the sec-

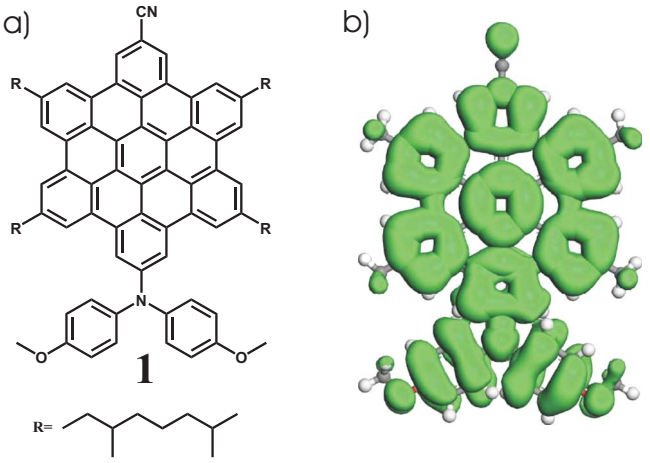

FIG. 1. (Color online) (a) Molecular structure of 2-cyano-11-[bis-(4′-methoxylphenyl)-amino]-5,8,14,17-tetra (3′, 7′-dimethyloctyl)-hexa-*peri*-hexabenzocoronene. (b) Sum of the electron densities of the four highest-occupied molecular orbitals, which lie within 1 eV to the HOMO (Ref. 12). For clarity, the side chains are replaced with methyl groups since electron-density calculations were not influenced significantly by the replacement.

ond layer contrast upon bias reduction [Figs. 2(c) and 2(d)] does not suggest its destabilization. Interestingly, imaging at the positive sample bias reverses the bias-dependent visibility of the molecular layers (Fig. 3). Imaging at low positive sample biases reveals dimer layers. Increase in the positive sample bias renders the dimer layer apparently less visible and the first oblique layer becomes more pronounced. Imaging of the same area under biases of different values and signs demonstrates again that the molecular layers remain physically unperturbed but their visibility varies.[12]

The dependence of the visibility of the molecular layers on the applied bias indicates that the bias influences the conditions for the resonant tunneling through the respective layers. We attribute this to the fact that the conditions for the resonant tunneling can depend on the relative position of the molecule in the tip-sample gap.[14–17] Let us assume that the tip and the surface are both planar electrodes. Second, we assume that the molecular layers do not affect the potential drop, i.e., for instance, they are not charged. In this case the energy of the orbitals will depend linearly on the position of the molecules between the electrodes.[17] The assumption that the potential decreases linearly facilitates the following discussion but it is not essential. Let us assume further that the electronic structures of the molecules in both layers are identical. Indeed, it has been demonstrated that the interaction of alkylated nanographenes with HOPG is relatively weak such that largely unperturbed electron orbitals can be observed with STM.[14,15] High-resolution STM images of the first layer [Fig. 2(b)] suggest again little influence of the substrate on the molecular orbitals. Based on the above assumptions a bias variation will affect the energy of the electron orbitals of the molecules in different layers differently (Fig. 4), such that resonant tunneling through the HOMO of the first layer is accomplished at lower bias in comparison with the bias required to tunnel through the HOMO of the molecules in the second layer. Both layers become visible, when a resonant tunneling condition is achieved for the second layer. Application of positive sample bias reverses the situation. Resonant tunneling conditions are fulfilled for the first layer at a lower bias and at high bias both layers should become visible. Obviously, the simple model provides an adequate description of the experimental observations.

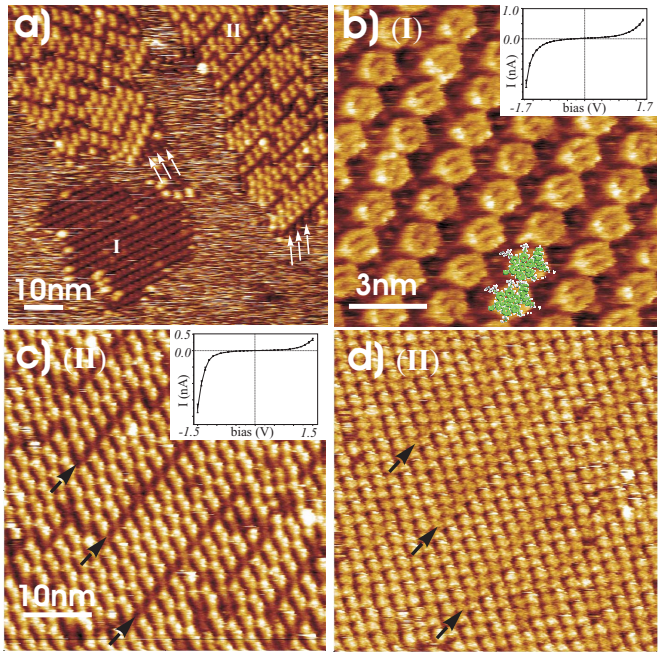

FIG. 2. (Color online) STM height images of molecular layers of **1** on HOPG. (a) Large-scale image (U_t=−1.3 V and I_t=61 pA) demonstrates two different types of structures: (I) regular oblique packing and (II) dimers, which include also a large number of structural defects such as missing molecules. Apparently dimers (II) grow on top of the oblique structure (I), which can be recognized below the structure of the dimers as indicated with the arrows. (b) Image of structure (I) (U_t=−0.91 V and I_t=41 pA); insert displays $I(U)$ dependence (taken at the tip-surface distance defined by the U_t=−0.69 V and I_t=41 pA feedback parameters). The suggested orientation of the molecules is depicted with the two HOMOs. (c) Image of structure (II) (U_t=−1.21 V and I_t=41 pA); insert displays $I(U)$ dependence (taken at the tip-surface distance defined by the U_t=−0.69 V and I_t=41 pA feedback parameters); a few examples of rows of missing molecules in the second layer are indicated with the arrows. (d) Image of the same area as in (c) recorded at a lower negative sample bias (U_t=−0.91 V and I_t=41 pA), the regular structure of the first layer is more apparent; however the second layer can be still recognized, for example, the same rows of missing molecules as in (c) are indicated with arrows.

A quantitative description has to be more elaborate. For example, we do not know the absolute distance between the tip and the second molecular layer. The tip-surface distance defines the potential decay (Fig. 4) and the corresponding conditions for resonant tunneling. It is reasonable to assume that the molecular layers are offset closer to the surface than to the tip, and asymmetric current-voltage characteristics agree with this assumption. The tip-surface distance can vary from tip to tip[18] and within one experiment for different bias-current settings. The tip-surface distance varies even within one image; however these variations are small, i.e., 0.5 and

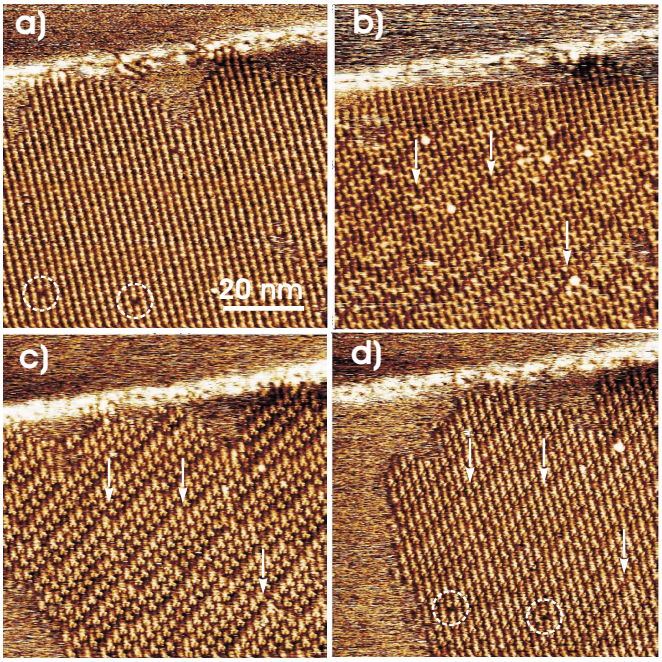

FIG. 3. (Color online) STM height images of the same spot made under different scanning parameters. (a) U_t=−0.713 V and I_t=0.048 nA, (b) U_t=−1.185 V and I_t=0.056 nA, (c) U_t=+0.559 V and I_t=0.046 nA, and (d) U_t=+0.743 V and I_t=0.053 nA. The large line defect in the upper part of the image is the graphene step edge. Arrows indicate same defects in the dimer layer well visible at high negative and low positive sample biases. Dashed circles underline missing molecules in the oblique structure well visible at low negative or high positive biases.

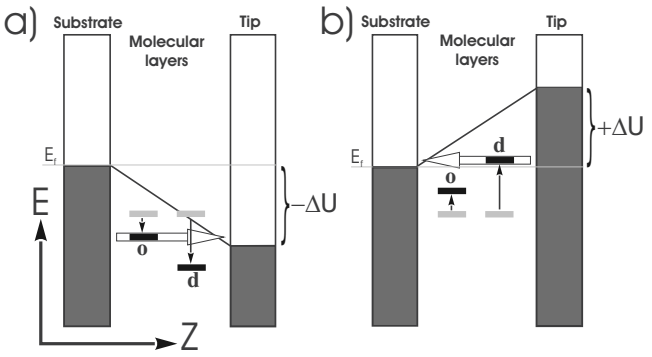

FIG. 4. Diagram illustrating the proposed explanation for the observed bias-dependent imaging of the molecular double layer. The axes of the diagram are distance (Z) in the direction between tip and surface and energy (E). The gray thick lines indicate HOMOs of two molecular layers, thin gray lines indicate Fermi levels (E_f) of unbiased tip and substrate. (a) Application of a negative substrate bias causes electrons to tunnel from the filled states of the sample (blackened area) to the unfilled states of the tip. Potential drop between substrate and tip shifts the HOMOs (to black thick lines) of both molecular layers, however the HOMO of the molecules in the first layer arranged into the oblique structures (o) is shifted more in comparison with the HOMO of the molecules arranged in the dimmer (d) structures in the second layer, thus resonant tunneling (indicated with the arrow) through (o) layer is accomplished at a lower negative bias compared with (d) layer. (b) Application of positive bias mirrors the situation, such that resonant tunneling through layer (d) is accomplished at a lower positive bias.

1.5 Å maximum apparent height difference between first and second layers in Figs. 3(b) and 3(c), respectively. The variation is small in comparison to the intermolecular layer distance, which should be larger than the interlayer distance in HOPG (3.35 Å, taking into account that **1** can be considered as tiny graphenes). Thus the simple model remains valid. Continuous-imaging tunneling spectroscopy[19] would be potentially more suitable for demonstration of bias-dependent imaging, however it requires a relatively long time to acquire an image which was troublesome in our case due to thermal drifts. Instead we used highest possible set-point currents for stable imaging for different biases, which should position the tip as close as possible to the molecular layers.

Images taken at large positive and negative biases are not identical. Both layers can be recognized, however the second layer is more pronounced at large negative [Fig. 3(b)] while the first layer can be better recognized at large positive [Fig. 3(d)] biases. We would like to point out that even the simple model (Fig. 4) suggests an inequality of the tunneling probability through the first and the second layers at large biases because of the difference in the potential barrier heights and the distance to the Fermi level for the HOMOs of the molecules in the first and second molecular layers.

Furthermore the potential drop can deviate from linearity due to the nonplanarity of the tip shape and also because of charge transfer to the molecular layers. Charging of the molecular layer was proposed as the explanation for the dependence of the current-voltage curves on the relative position of the molecules in the tip-substrate gap[20] since charging of the molecules and the associated shifts of their orbitals were argued to depend on the relative position of the molecule between tip and substrate. However, we do not see how to employ these arguments in order to explain the experimental results reported here for the double layer while the explanation based on the proposed dependence of molecular-orbital energies on the relative position of the molecules in the gap between tip and substrate is quite straightforward.

In summary, we investigated bias-dependent imaging of a molecular double layer of a nanographene on graphite. The different structure of the first and second layers allowed us to monitor the visibility of the two layers at different biases. We found that the second layer can be visualized at high negative and low positive sample biases while the first layer can be visualized at low negative and high positive sample biases. We explain this effect with a different dependence of the energy of the molecular orbitals upon bias variation for molecules located at different positions within the tip-substrate gap. The generic nature of the results' interpretation suggests similar behavior for other molecules weakly coupled with substrates,[21,22] especially in the case of large molecule-substrate distances. It implies that imaging of occupied and unoccupied states can be achieved at both bias polarities.[23] The concept can be extended straightforward to multilayer systems. Upon continuous bias increase, the image of each subsequent layer reaches conditions for resonant

tunneling, which suggests the possibility of an "STM tomography" of molecular multilayers.

This work was supported by the DFG through SFB 658 "Elementary processes in molecular switches at surfaces" and by the Max Planck Society through the program ENERCHEM, the German Science Foundation (Korean-German IRTG) and DFG Priority Program SPP 1355, also financial support by the European Community project "IControl" (Contract No. EC-STREP-033197) is gratefully acknowledged. The authors would like to thank Georg Heimel (HU) for fruitful discussions.

*Author to whom correspondence should be addressed.
†nikolai.severin@physik.hu-berlin.de
‡rabe@physik.hu-berlin.de

[1] H. Ohtani, R. J. Wilson, S. Chiang, and C. M. Mate, Phys. Rev. Lett. **60**, 2398 (1988).
[2] J. P. Rabe and S. Buchholz, Science **253**, 424 (1991).
[3] D. Braun, A. Schirmeisen, and H. Fuchs, Surf. Sci. **575**, 3 (2005).
[4] P. Guaino, D. Carty, G. Hughes, O. McDonald, and A. A. Cafolla, Appl. Phys. Lett. **85**, 2777 (2004).
[5] F. Jäckel, M. Ai, J. Wu, K. Müllen, and J. P. Rabe, J. Am. Chem. Soc. **127**, 14580 (2005).
[6] F. Jäckel, M. D. Watson, K. Müllen, and J. P. Rabe, Phys. Rev. B **73**, 045423 (2006).
[7] M. M. Reiter, F. Jamitzky, F. Trixler, and W. M. Heckl, Phys. Status Solidi A **187**, 171 (2001).
[8] P. Samorí, N. Severin, C. D. Simpson, K. Müllen, and J. P. Rabe, J. Am. Chem. Soc. **124**, 9454 (2002).
[9] A. Cristadoro, M. Ai, H. J. Rader, J. P. Rabe, and K. Müllen, J. Phys. Chem. C **112**, 5563 (2008).
[10] X. Dou, X. Feng, and K. Müllen (unpublished).
[11] K. Besocke, Surf. Sci. **181**, 145 (1987).
[12] See EPAPS Document No. E-PRBMDO-80-028948 for the complete sequence of STM height images, partially displayed in Fig. 2. For more information on EPAPS, see http://www.aip.org/pubservs/epaps.html.
[13] T. Böhme, C. D. Simpson, K. Müllen, and J. P. Rabe, Chem. Eur. J. **13**, 7349 (2007).
[14] F. Jäckel, Z. Wang, M. D. Watson, K. Müllen, and J. P. Rabe, Chem. Phys. Lett. **387**, 372 (2004).
[15] A. Stabel, P. Herwig, K. Müllen, and J. P. Rabe, Angew. Chem., Int. Ed. Engl. **34**, 1609 (1995).
[16] P. E. Kornilovitch, A. M. Bratkovsky, and R. S. Williams, Phys. Rev. B **66**, 165436 (2002).
[17] W. Mizutani, M. Shigeno, K. Kajimura, and M. Ono, Ultramicroscopy **42-44**, 236 (1992).
[18] S. W. Hla, V. Marinkovic, A. Prodan, and I. Musevic, Surf. Sci. **352-354**, 105 (1996).
[19] R. J. Hamers, R. M. Tromp, and J. E. Demuth, Phys. Rev. Lett. **56**, 1972 (1986).
[20] T. G. Gopakumar, F. Müller, and M. Hietschold, J. Phys. Chem. B **110**, 6060 (2006).
[21] J. Repp, G. Meyer, S. M. Stojkovic, A. Gourdon, and C. Joachim, Phys. Rev. Lett. **94**, 026803 (2005).
[22] X. W. Tu, G. R. Mikaelian, and W. Ho, Phys. Rev. Lett. **100**, 126807 (2008).
[23] S. B. Lei, C. Wang, S. X. Yin, Q. M. Xu, and C. L. Bai, Surf. Interface Anal. **32**, 253 (2001).